



Alpha/proton Instability in the Presence of Proton and Alpha Temperature Anisotropy and its Application to the Deceleration of Alpha Particles in the Solar Wind

Wen-Lu Zhang¹, Liang Xiang^{1,2}, Qiu-Huan Li², Si-Yi Lang¹, and Hong-Wei Yu¹

¹ Department of Physics and Synergetic Innovation Center for Quantum Effects and Applications, School of Physics and Electronics, Hunan Normal University, Changsha 410081, China; hwyu@hunnu.edu.cn

² Institute of Space Physics, Luoyang Normal University, Luoyang 471934, China; xiangliang@hunnu.edu.cn
Received 2021 August 24; revised 2021 September 15; accepted 2021 October 3; published 2022 January 21

Abstract

Observations of solar wind plasma find that the drift velocity between alpha beams and protons, v_α , is reduced with the heliocentric distance, but the ratio of v_α to v_A (the local Alfvén velocity) does not vary obviously and has a typical velocity ratio of $v_\alpha/v_A \leq 1$. The alpha beam instability is believed to be responsible for the deceleration of alpha beams in the solar wind. However, the role of the temperature anisotropy of ions (protons and alpha particles) on the alpha beam instability has not been examined. Based on the kinetic theory of the PDRK solver, this study systemically investigates the alpha beam instability in the presence of proton and alpha temperature anisotropies and considers the effects of these temperature anisotropies on the instability at an arbitrary propagation angle relative to the ambient magnetic field. It is found that the real frequencies, growth rates and threshold conditions of the excited waves sensitively depend on the proton temperature anisotropy $T_{i\perp}/T_{i\parallel}$ and the alpha temperature anisotropy $T_{\alpha\perp}/T_{\alpha\parallel}$, as well as the parallel electron beta $\beta_{e\parallel}$. In particular, for both alpha beam and proton temperature anisotropy driven cases, the parallel magnetosonic/whistler (PM/W), backward magnetosonic/whistler (BM/W) and oblique Alfvén/ion cyclotron (OA/IC) waves arise when $T_{i\perp}/T_{i\parallel} < 1$, and the PM/W, OA/IC, parallel Alfvén/ion cyclotron (PA/IC) and mirror waves occur when $T_{i\perp}/T_{i\parallel} > 1$. The presence of anisotropic protons leads to a lower velocity threshold for the OA/IC and BM/W waves at $T_{i\perp}/T_{i\parallel} < 1$ and for the OA/IC, PA/IC and mirror waves at $T_{i\perp}/T_{i\parallel} > 1$. For both alpha beam and alpha temperature anisotropy driven cases, the PM/W and OA/IC waves are unstable when $T_{\alpha\perp}/T_{\alpha\parallel} < 1$, and the PM/W, OA/IC, PA/IC, oblique magnetosonic/whistler (OM/W) and mirror waves are likely to grow as $T_{\alpha\perp}/T_{\alpha\parallel} > 1$. The presence of anisotropic alpha particles results in a lower threshold velocity for the PM/W wave at $T_{\alpha\perp}/T_{\alpha\parallel} < 1$ and for the PA/IC, OM/W and mirror waves at $T_{\alpha\perp}/T_{\alpha\parallel} > 1$. On account of the influences of the anisotropic proton and alpha, these alpha beam instabilities can effectively constrain the alpha-beam drift velocity to less than or equal to the local Alfvén velocity. These results may shed light on the evolution and deceleration mechanism of alpha particles in the solar wind.

Key words: (Sun:) solar wind – Sun: heliosphere – waves

1. Introduction

Observations from Helios, Wind and PSP spacecraft have revealed that alpha particles are omnipresent in the solar wind (Bame et al. 1977; Pizzo et al. 1983; Marsch & Richter 1984; Li & Li 2006). The alpha particles comprise about 5% of ions and they stream faster than the ambient protons (Steinberg et al. 1996; Neugebauer et al. 1996; Feldman et al. 1996). The drift velocity of the alpha beams with respect to the ambient solar wind is usually equal to or less than the local Alfvén velocity, and these beams propagate in directions nearly parallel to the ambient magnetic field (Marsch & Livi 1987; Verniero et al. 2020). In the weakly collisional plasma environment of the solar wind, the alpha beams are typically at a higher temperature than the background protons by a factor of around

four or even larger (Ebert et al. 2009; Borovsky 2016). The local Alfvén velocity of solar wind will decrease with the heliocentric distance when propagating from the Sun into the interplanetary space, and the limitation of the alpha beam drift velocity implies a continuous deceleration of the alpha beams throughout the whole interplanetary space (Kasper et al. 2008; Bourouaine et al. 2013; Āurovcová et al. 2019). Moreover, these alpha particles play a particularly important role in the energization processes of particles in the solar wind (Chandran et al. 2013; Verscharen et al. 2015; Ofman 2019; Markovskii et al. 2019). However, the formation and evolution mechanism of the alpha particles in the solar wind are still unclear.

The drift velocity of the alpha beams, if it is large enough, can excite two different types of electromagnetic alpha/proton modes: the magnetosonic/whistler wave and the Alfvén/

ion-cyclotron wave (Revathy 1978; Verscharen et al. 2013a, 2013b). The former is prior to generate in the plasma with $\beta > 1$, and it propagates along the ambient magnetic field \mathbf{B}_0 , where β is the ratio of plasma thermal to magnetic pressures (Gary et al. 2000a, 2000b). The latter is inclined to arise in the plasma with $\beta < 1$, and it is oblique to the \mathbf{B}_0 field. These alpha beam instabilities are believed to be an efficient mechanism in constraining the beam velocity (Lu et al. 2009; Rehman et al. 2020). As soon as the threshold condition is satisfied, the corresponding wave is effectively induced, which leads to an exchange of energy between energetic beams and waves via the wave-particle interactions, and the beam drift velocity decreases (Gary et al. 2001; Xiang et al. 2018). In this way, these instabilities can put an upper bound on the alpha-beam drift velocity. However, the observed alpha-beam drift velocity is far less than the theoretical prediction (Reisenfeld et al. 2001; Bourouaine et al. 2013).

On the other hand, ions usually present a bi-Maxwellian velocity distribution in the solar wind, which can be represented as different temperature components $T_{\perp} \neq T_{\parallel}$ with respect to \mathbf{B}_0 , such as the proton temperature anisotropy $T_{i\perp}/T_{i\parallel}$ (Kasper et al. 2003; Bale et al. 2009; Maruca et al. 2012; Seough et al. 2013; Huang et al. 2020; Hellinger et al. 2006) and the alpha temperature anisotropy $T_{\alpha\perp}/T_{\alpha\parallel}$ (Marsch et al. 1982b; Gary et al. 2016). Due to the propagating-wind expansion, the perpendicular and parallel temperature components can be governed by the CGL mechanism (Chew et al. 1956). In some plasma environments with $T_{i\perp} \neq T_{i\parallel}$, the value of $T_{i\perp}/T_{i\parallel}$ is often located in the range of 1 to 2 in the fast wind, while it is less than 0.5 in the slow solar wind (Marsch et al. 1982a; Marsch 2012; Jian et al. 2016). In addition, in some plasma environments with $T_{\alpha\perp} \neq T_{\alpha\parallel}$, the value of $T_{\alpha\perp}/T_{\alpha\parallel}$ is smaller than 1 in the slow wind, and sometimes it is larger than 1 in the fast solar wind (Gary et al. 2016). Therefore, the temperature anisotropies of both proton and alpha can be smaller or larger than 1 in different solar wind plasma environments.

In the previous studies of Gary et al. (2000a, 2000b), the linear theory and hybrid simulations were used to study the growing modes of the alpha beam instability and the role of the wave-particle scattering on the ion heating and acceleration. However, their studies examined the properties of the alpha beam instability in simple Maxwellian or drift-Maxwellian plasmas. In this study, we investigate the alpha beam instability in the presence of anisotropic proton and alpha and analyze the effects of proton and alpha temperature anisotropies on these instabilities at arbitrary propagation angles relative to \mathbf{B}_0 . Our present results can provide a physical mechanism to explain the deceleration of alpha beams in the solar wind. The rest of this paper is organized as follows. In Section 2, the basic model and the Vlasov equation are presented. In Section 3, we investigate the effects of the proton temperature anisotropy on the alpha beam instability. In Section 4, we also study the effects of the

alpha temperature anisotropy on the alpha beam instability. Finally, in Section 5, the discussion and conclusion are given.

2. Plasma Model and Wave Equation

In the alpha-beam return-current system magnetized by the background magnetic field $\mathbf{B}_0 = B_0 \mathbf{e}_z$, let us consider a collisionless plasma with three particle species: the static proton (i) with anisotropic temperatures, the alpha beam (α) with anisotropic temperatures and field-aligned drift velocity v_{α} , and the background electron (e) with isotropic temperatures and field-aligned drift velocity v_e . Taking into account both the beam and temperature anisotropy, the equilibrium distribution function, which is assumed in the drift bi-Maxwellian distribution, can be given as follows (Chen & Wu 2012):

$$f_{s0} = \frac{n_s}{(2\pi)^{3/2} v_{T_{s\perp}}^2 v_{T_{s\parallel}}} e^{-\frac{v_{\perp}^2}{2v_{T_{s\perp}}^2} - \frac{(v_{\parallel} - v_s)^2}{2v_{T_{s\parallel}}^2}}, \quad (1)$$

where n_s and v_s represent the number density and the drift velocity for species s , respectively. The subscripts $s = i, \alpha$ and e denote the ambient proton, alpha beam and ambient electron, respectively, and the subscripts \perp and \parallel correspond to the perpendicular and parallel directions with respect to \mathbf{B}_0 . Here $v_{\perp} = \sqrt{v_x^2 + v_y^2}$ and $v_{\parallel} = v_z$ represent the perpendicular and parallel velocities, respectively. While $v_{T_{s\perp(\parallel)}} = \sqrt{\frac{T_{s\perp(\parallel)}}{m_s}}$ is the perpendicular (parallel) thermal velocity, and m_s and $T_{s\perp(\parallel)}$ represent the mass and the perpendicular (parallel) temperature, respectively.

In collisionless space and astrophysical plasmas, waves and instabilities can be derived from the following equations (Wu 2012)

$$\begin{aligned} & \left[\frac{\partial}{\partial t} + \mathbf{v} \cdot \nabla + \frac{q_s}{m_s} (\mathbf{v} \times \mathbf{B}_0) \cdot \nabla \right] f_{s1} \\ & = -\frac{q_s}{m_s} (\mathbf{E}_1 + \mathbf{v} \times \mathbf{B}_1) \cdot \nabla f_{s0}, \\ & \nabla \times \mathbf{B}_1 = \mu_0 \mathbf{j} + \frac{1}{\varepsilon_0 \mu_0} \frac{\partial \mathbf{E}_1}{\partial t}, \\ & \nabla \times \mathbf{E}_1 = -\frac{\partial \mathbf{B}_1}{\partial t}, \end{aligned} \quad (2)$$

where q_s , f_{s0} , and f_{s1} represent the charge, unperturbed distribution function, and perturbed distribution function. \mathbf{E}_1 and \mathbf{B}_1 are the electric field fluctuation and magnetic field fluctuation, respectively.

By combining Equations (1) and (2), the general dispersion relation in a homogeneous plasma can be obtained as follows (Stix 1992)

$$\begin{vmatrix} \varepsilon_{xx} - c^2 k_z^2 / \omega^2 & \varepsilon_{xy} & \varepsilon_{xz} + c^2 k_x k_z / \omega^2 \\ \varepsilon_{yx} & \varepsilon_{xx} - c^2 k^2 / \omega^2 & \varepsilon_{yz} \\ \varepsilon_{zx} + c^2 k_x k_z / \omega^2 & \varepsilon_{zy} & \varepsilon_{zz} - c^2 k_x^2 / \omega^2 \end{vmatrix} = 0, \quad (3)$$

where

$$\varepsilon = I + \sum_s \frac{\omega_{ps}^2}{\omega^2} \sum_n \left[\zeta_{s0} Z(\zeta_{sn}) - \left(1 - \frac{T_{s\perp}}{T_{s\parallel}} \right) \right] (1 + \zeta_{sn} Z(\zeta_{sn})) Y_{sn} + \sum_s \frac{2\omega_{ps}^2}{\omega^2} \zeta_{s0} \frac{T_{s\parallel}}{T_{s\perp}} e_z e_z, \quad (4)$$

and

$$Y_{sn} = \begin{bmatrix} n^2 \Gamma_{sn} / \lambda_s & in \Gamma'_{sn} & -n \left(\frac{T_{s\parallel}}{T_{s\perp}} \right)^{1/2} \frac{\omega + n\omega_{cs}}{k_z v_{T_{s\parallel}}} \Gamma_{sn} / \sqrt{\lambda_s} \\ -in \Gamma'_{sn} & n^2 \Gamma_{sn} / \lambda_s - 2\lambda_s^2 \Gamma'_{sn} & i \left(\frac{T_{s\parallel}}{T_{s\perp}} \right)^{1/2} \frac{\omega + n\omega_{cs}}{k_z v_{T_{s\parallel}}} \sqrt{\lambda_s} \Gamma'_{sn} \\ -n \left(\frac{T_{s\parallel}}{T_{s\perp}} \right)^{1/2} \frac{\omega + n\omega_{cs}}{k_z v_{T_{s\parallel}}} \Gamma_{sn} / \sqrt{\lambda_s} - i \left(\frac{T_{s\parallel}}{T_{s\perp}} \right)^{1/2} \frac{\omega + n\omega_{cs}}{k_z v_{T_{s\parallel}}} \sqrt{\lambda_s} \Gamma'_{sn} & \frac{\omega + n\omega_{cs}}{k_z v_{T_{s\parallel}}} \sqrt{\lambda_s} \Gamma'_{sn} & \left(\frac{T_{s\parallel}}{T_{s\perp}} \right) \frac{(\omega + n\omega_{cs})^2}{k_z^2 v_{T_{s\parallel}}^2} \Gamma_{sn} \end{bmatrix}. \quad (5)$$

In the above expressions, $\lambda_s = \frac{k_x^2 v_{T_{s\perp}}^2}{\omega_{cs}^2}$, $\zeta_{s0} = \frac{\omega - k_z v_s}{\sqrt{2} k_z v_{T_{s\parallel}}}$, $\zeta_{sn} = \frac{\omega - k_z v_s - n\omega_{cs}}{\sqrt{2} k_z v_{T_{s\parallel}}}$, $\omega_{cs} = \frac{q_s B_0}{m_s}$, $\omega_{ps} = \sqrt{\frac{n_{s0} q_s^2}{\varepsilon_0 m_s}}$, and $\Gamma_{sn} = I_n(\lambda_s) e^{-\lambda_s}$.

Here $I_n(\lambda_s)$ is the modified Bessel function of the first kind of n th-order, and $Z(\zeta_{sn})$ is the plasma dispersion function. Under the plane wave assumption, the wavevector is $\mathbf{k} = k_x \mathbf{e}_x + k_z \mathbf{e}_z$. From nontrivial solutions of Equation (3), all plasma modes in arbitrary directions relative to \mathbf{B}_0 can be derived in the kinetic Valsov system.

Several numerical methods were developed to solve the kinetic dispersion relation of Equation (3), such as WHAMP (Roennmark 1982), NHDS (Verscharen et al. 2013b) and KUPDAP (Sugiyama et al. 2015). In this study, we adopt a new numerical solver, PDRK (Xie & Xiao 2016; Xie 2019), to find the dispersion relation of the plasma modes in Equation (3). Unlike other solvers by using the Newton iterative method, the PDRK solver is based on the standard matrix eigenvalue method to solve an equivalent linear equation system that was derived from the linear transformation of Equation (3). Therefore, all physical solutions can be obtained by running the PDRK solver without requiring any initial guess value, which provides an excellent opportunity to examine the plasma instability. Recently, using the PDRK solver, several plasma instabilities have been investigated in various active phenomena in space and solar plasmas, including the proton and

electron temperature anisotropy (Sun et al. 2019, 2020) and the proton beam instability (Xiang et al. 2020, 2021) in the solar wind, and the electron beam instability in flare loops (Chen et al. 2020).

In the numerical calculations, we assume both the charge-neutral and zero-current conditions in the alpha beam-return current system, i.e., $\sum_s q_s n_s = 0$ and $\sum_s q_s n_s v_s = 0$. We also perform calculations in the center of the background-proton frame. The plasma parameters $n_e = 5 \times 10^6 \text{ m}^{-3}$, $B_0 = 5 \times 10^{-9} \text{ T}$, and $4T_{i\parallel} = 4T_{e\parallel} = T_{\alpha\parallel}$ have been adopted. Here both the background proton and the alpha beam with temperature anisotropies are considered, $T_{i\perp} \neq T_{i\parallel}$ and $T_{\alpha\perp} \neq T_{\alpha\parallel}$, while the background electron is assumed to be isotropic, $T_{e\perp} = T_{e\parallel}$.

3. Effects of Proton Temperature Anisotropy on Alpha Beam Instability

In this section, we investigate the wave dispersion and polarization properties of the alpha beam instability accompanied with the proton temperature anisotropy and systematically analyze the influences of the proton temperature anisotropy on the wave frequency, growth rate and threshold condition.

Figure 1 displays the distribution of the dispersion relation and polarization properties in the plane of the propagation angle θ and normalized wavenumber $k\lambda_i$ for the oblique Alfvén/ion-cyclotron (OA/IC) wave in the plasma with low-beta $\beta_{e\parallel} = 0.1$ ($\beta_{e\parallel} = 2\mu_0 n_e T_{i\parallel} / B_0^2$ being the parallel electron beta), where panels (a), (b) and (c) correspond to different proton temperature anisotropies $T_{i\perp} / T_{i\parallel} = 0.25, 1$ and 2 , respectively. The plasma parameters are $n_\alpha / n_e = 0.05$, $v_\alpha / v_A = 1.5$, $T_{\alpha\parallel} = 4T_{e\parallel} = 4T_{i\parallel}$ and $T_{\alpha\perp} = 4T_{e\perp} = 4T_{i\perp}$. As can be seen from Figure 1, the proton beam can effectively drive the OA/IC wave in the low-beta case, i.e., $\beta_{e\parallel} = 0.1$, and its propagation angle is located in the region of $30^\circ \leq \theta \leq 70^\circ$. Moreover, as the proton temperature anisotropy $T_{i\perp} / T_{i\parallel}$ increases from 0.25 to 2, the OA/IC wave properties of ω_r / ω_{ci} , γ / ω_{ci} and E_y / iE_x do not vary obviously.

Figure 2 shows the distribution of the dispersion relations and polarization properties in the plane of the propagation angle θ and normalized wavenumber $k\lambda_i$ for the parallel magnetosonic/

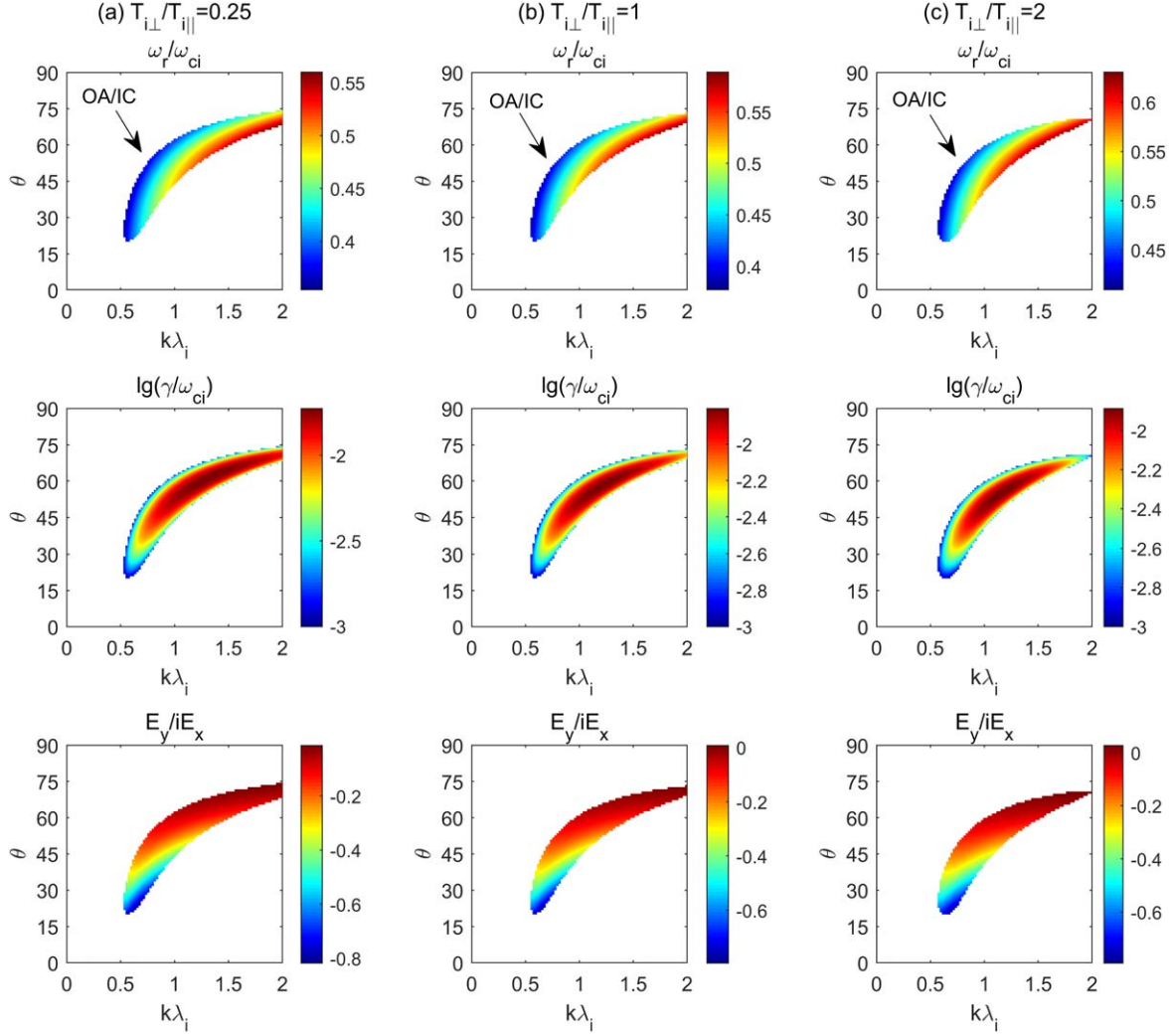


Figure 1. The distribution of the real frequency ω_r/ω_{ci} (top), growth rate γ/ω_{ci} (middle) and polarization E_y/iE_x (bottom) in the plane of the propagation angle θ and normalized wavenumber $k\lambda_i$ for the OA/IC wave in the plasma with low-beta $\beta_{e\parallel} = 0.1$, where the left, middle and right panels correspond to different proton temperature anisotropies of (a) $T_{i\perp}/T_{i\parallel} = 0.25$, (b) 1 and (c) 2. The additional plasma parameters $n_\alpha = 0.05n_e$, $v_\alpha = 1.5v_A$, $T_{\alpha\parallel} = 4T_{e\parallel} = 4T_{i\parallel}$ and $4T_{e\perp} = T_{\alpha\perp} = 4T_{i\perp}$ have been used.

whistler (PM/W), backward magnetosonic/whistler (BM/W), parallel Alfvén/ion-cyclotron (PA/IC), OA/IC and mirror waves in the plasma with high-beta $\beta_{e\parallel} = 1.5$. Here planes (a), (b) and (c) correspond to different proton temperature anisotropies $T_{i\perp}/T_{i\parallel} = 0.25$, 1 and 2, respectively. Other plasma parameters are the same as Figure 1. From Figure 2, it can be found that in the case of $\beta_{e\parallel} = 1.5$ and $T_{i\perp}/T_{i\parallel} = 1$, the alpha beams can drive both the PM/W and OA/IC waves, which correspond to different propagation angles $\theta \leq 10^\circ$ and $40^\circ \leq \theta \leq 65^\circ$, respectively. As $T_{i\perp}/T_{i\parallel} = 0.25$, besides the PM/W and OA/IC waves, the proton temperature anisotropy provides an additional driving source to generate the BM/W wave in the direction of anti-parallel propagation. Compared to that of $T_{i\perp}/T_{i\parallel} = 1$, both the OA/IC and PM/W waves at $T_{i\perp}/T_{i\parallel} = 0.25$ have wider

propagation angle ranges for $20^\circ \leq \theta \leq 70^\circ$ and $\theta \leq 20^\circ$, respectively. As $T_{i\perp}/T_{i\parallel} = 2$, three kinds of modes exist, i.e., the PA/IC, OA/IC and mirror waves. The PA/IC, OA/IC and mirror waves dominate in different regimes of $\theta \leq 20^\circ$, $25^\circ \leq \theta \leq 55^\circ$ and $55^\circ \leq \theta < 90^\circ$, respectively.

In the following, the influences of the proton temperature anisotropy on the threshold conditions are also investigated. Figure 3 shows the distributions of the dispersion relations (ω_r/ω_{ci} and $\gamma_{\max}/\omega_{ci}$) in the plane of the parallel electron beta $\beta_{e\parallel}$ and the alpha-beam drift velocity v_α/v_A for different values of the proton temperature anisotropy $T_{i\perp}/T_{i\parallel} = 0.25$ ((a), (d)), 1 ((b), (e)) and 2 ((c), (f)). Here panels (a)–(c) represent the PM/W, BM/W and PA/IC waves at the parallel propagation case of $\theta = 0$, and panels (d)–(f) stand for the OA/IC and mirror

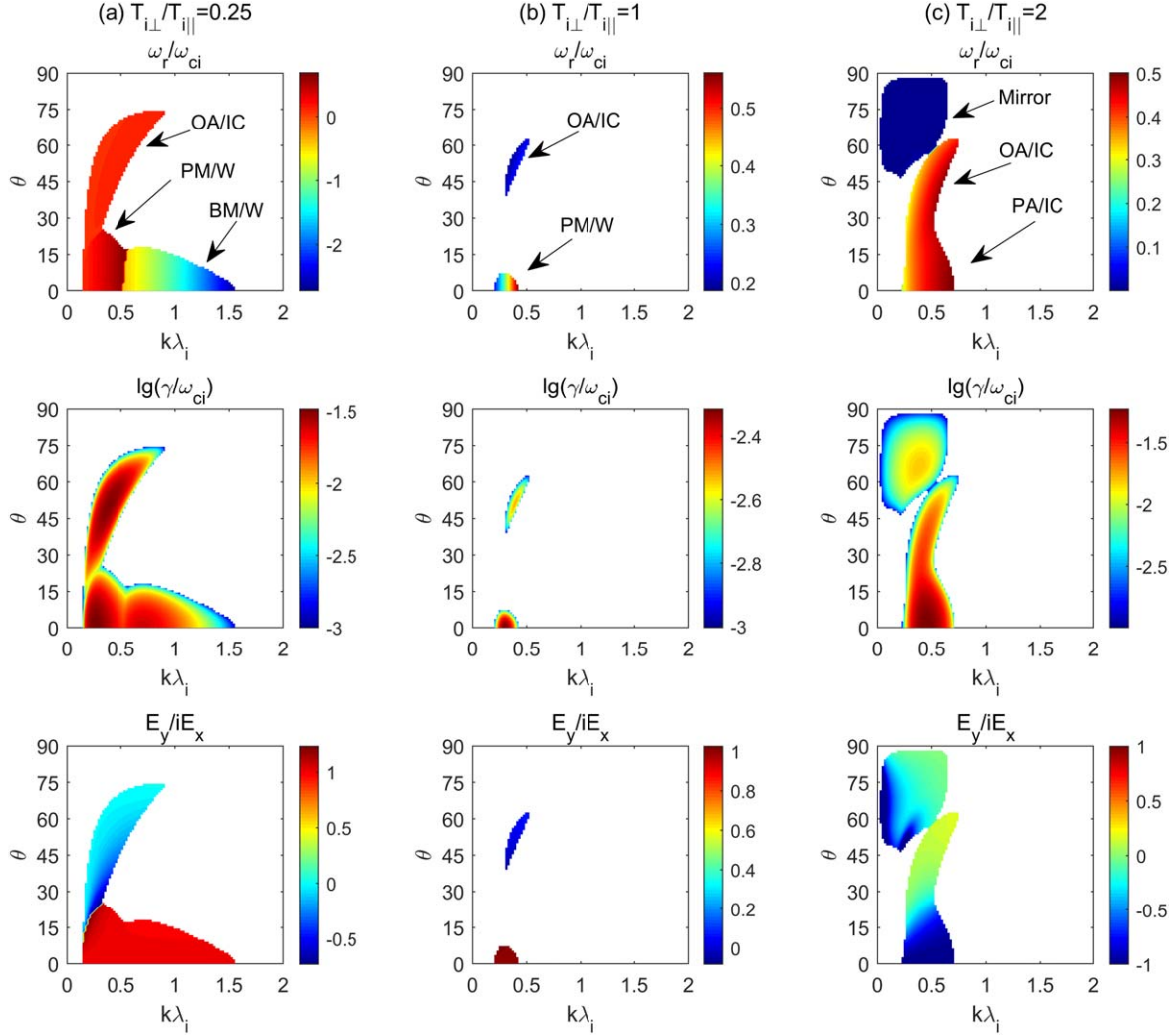


Figure 2. The distribution of the real frequency ω_r/ω_{ci} (top), growth rate γ/ω_{ci} (middle) and polarization E_y/iE_x (bottom) in the plane of the propagation angle θ and normalized wavenumber $k\lambda_i$ for the OA/IC, PM/W, BM/W, PA/IC and mirror waves in the plasma with high-beta $\beta_{e\parallel} = 1.5$, where the left, middle and right panels correspond to different proton temperature anisotropies of (a) $T_{i\perp}/T_{i\parallel} = 0.25$, (b) 1 and (c) 2. The additional plasma parameters $n_\alpha = 0.05n_e$, $v_\alpha = 1.5v_A$, $T_{\alpha\parallel} = 4T_{e\parallel} = 4T_{i\parallel}$ and $4T_{e\perp} = T_{\alpha\perp} = 4T_{i\perp}$ have been used.

waves at the oblique propagation case of $\theta = 55^\circ$. In the maximum growth rate distributions, the black solid lines correspond to the contour values of $\gamma_{\max}/\omega_{ci} = 10^{-3}$, 10^{-2} and 10^{-1} , and the curved line with $\gamma_{\max}/\omega_{ci} = 10^{-3}$ is defined as the instability threshold. Figure 3 clearly displays the dispersion relation and threshold distributions of the PM/W, BM/W, PA/IC, OA/IC and mirror waves, and their dependence on $\beta_{e\parallel}$ and v_α/v_A , as well as $T_{i\perp}/T_{i\parallel}$.

For parallel propagation cases ($\theta = 0$) shown in Figures 3(a)–(c), the velocity threshold and the real frequency of the PM/W wave decrease as $\beta_{e\parallel}$ increases in the absence of the proton temperature anisotropy, i.e., $T_{i\perp}/T_{i\parallel} = 1$. As $T_{i\perp}/T_{i\parallel} = 0.25$, the PM/W and BM/W waves can be generated, and the unstable region is enlarged obviously compared to the case of

$T_{i\perp}/T_{i\parallel} = 1$. In particular, the BM/W wave dominates in the unstable region at a smaller drift velocity of v_α/v_A , whereas the PM/W wave with a larger growth rate becomes very strong at a larger v_α/v_A . As $T_{i\perp}/T_{i\parallel} = 2$, both the PM/W and PA/IC waves are unstable, but they have different unstable regions. The threshold velocity v_α/v_A of the PA/IC wave is much smaller than that of the PM/W wave. For oblique propagation cases ($\theta = 55^\circ$) shown in Figure 3(d)–(f), only the OA/IC wave appears at $T_{i\perp}/T_{i\parallel} = 1$. As $T_{i\perp}/T_{i\parallel} = 0.25$, the threshold velocity of the OA/IC wave extends to a lower value (i.e., $v_\alpha/v_A < 1$), especially in the $\beta_{e\parallel} > 2$ regime. As $T_{i\perp}/T_{i\parallel} = 2$, both the OA/IC and mirror waves are induced in different v_α/v_A and $\beta_{e\parallel}$ regimes. The OA/IC wave with a larger growth rate tends to dominate in the unstable region at a larger v_α/v_A ,

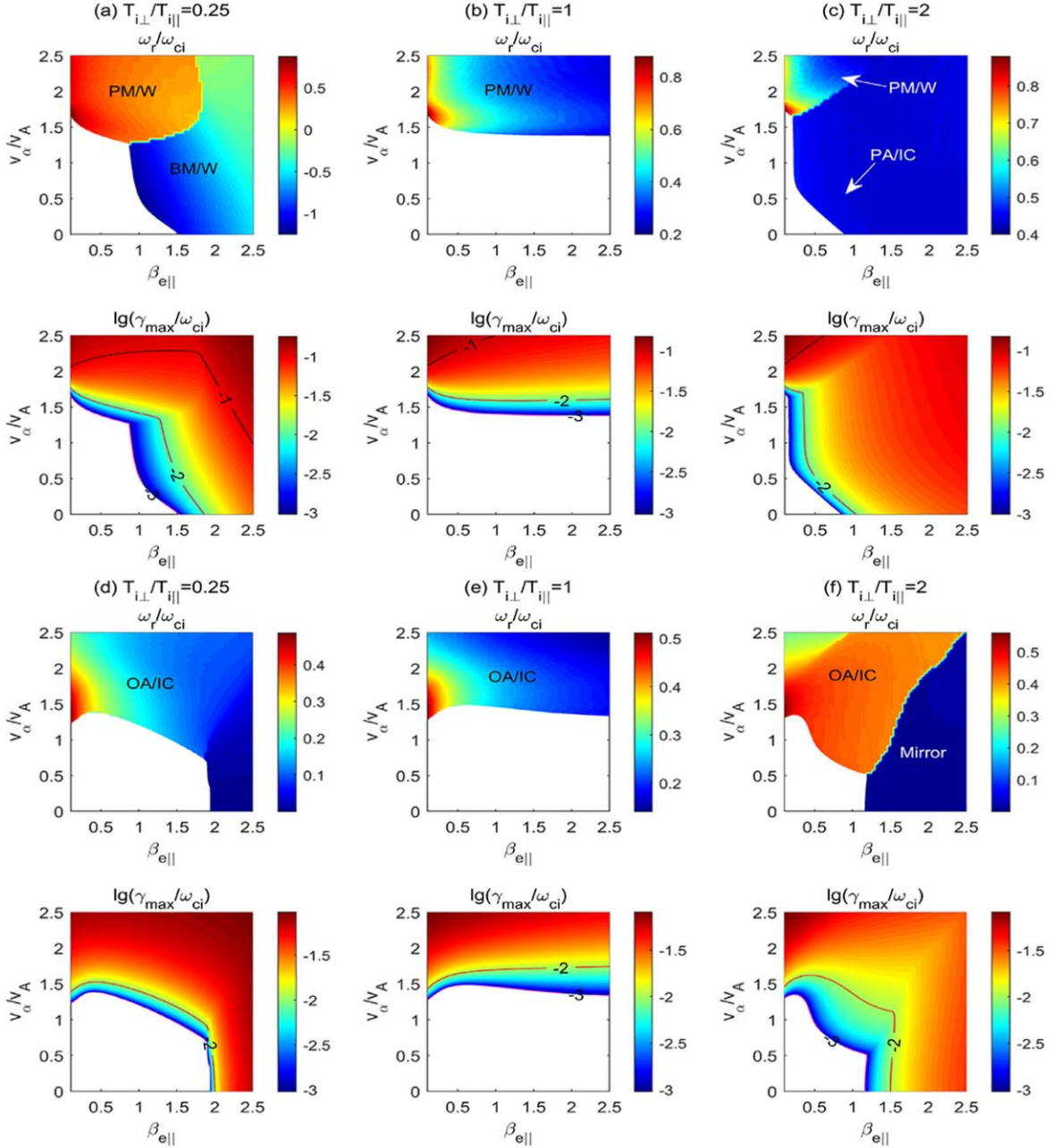


Figure 3. The distribution of the maximum growth rate $\gamma_{\max}/\omega_{ci}$ and corresponding real frequency ω_r/ω_{ci} in the plane of the parallel electron beta $\beta_{e\parallel}$ and alpha-proton drift velocity v_{α}/v_A for the PM/W, BM/W and PA/IC waves at $\theta = 0$ ((a)–(c)) and for the OA/IC and mirror waves at $\theta = 55^\circ$ ((d)–(f)). The left, middle and right panels correspond to different proton temperature anisotropies of $T_{i\perp}/T_{i\parallel} = 0.25$ ((a), (d)), 1 ((b), (e)) and 2 ((c), (f)). In the maximum growth rate panels, the values of $\gamma_{\max}/\omega_{ci} = 10^{-3}$, 10^{-2} and 10^{-1} are marked with the black solid line. The additional plasma parameters are $n_{\alpha} = 0.05n_e$, $T_{\alpha\parallel} = 4T_{e\parallel} = 4T_{i\parallel}$ and $4T_{e\perp} = T_{\alpha\perp} = 4T_{i\perp}$.

while the mirror wave with a lower threshold velocity is easily excited at a smaller v_{α}/v_A and a larger $\beta_{e\parallel}$.

The variations of instability thresholds with the alpha-beam drift velocity v_{α}/v_A and parallel electron beta $\beta_{e\parallel}$ are shown in Figure 4, where the top and bottom panels correspond to two different situations of (a) $T_{i\perp}/T_{i\parallel} \leq 1$ and (b) $T_{i\perp}/T_{i\parallel} \geq 1$,

respectively. In Figure 4(a) the solid, dotted and dashed lines correspond to the PM/W, BM/W and OA/IC waves, and in Figure 4(b) the solid, dotted, dashed and dotted–dashed lines represent the PM/W, PA/IC, OA/IC and mirror waves, respectively. For the cases of $T_{i\perp}/T_{i\parallel} \leq 1$ shown in Figure 4(a), there exist three kinds of waves: PM/W, OA/IC and BM/W

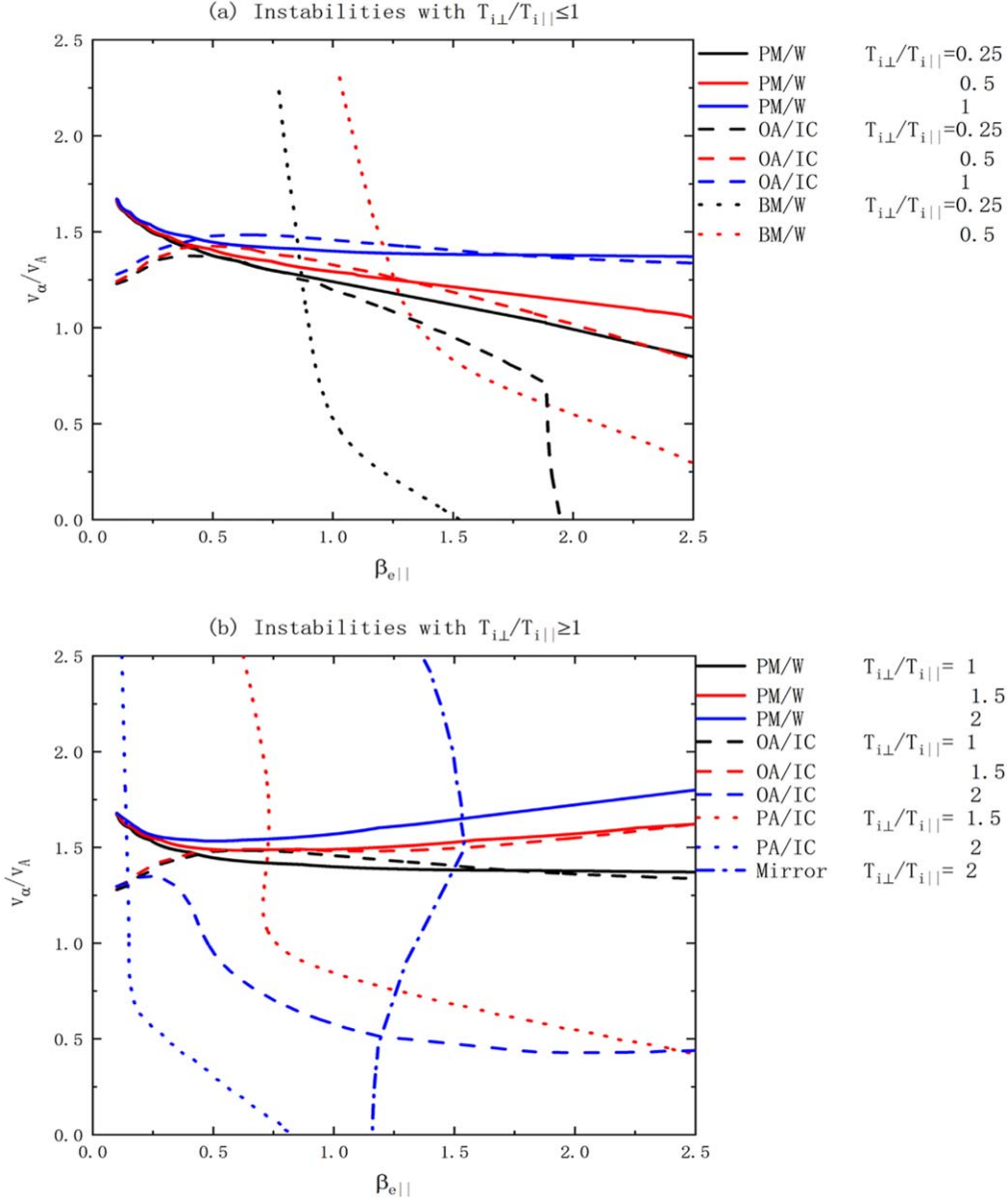


Figure 4. The instability threshold in the $\beta_{e\parallel} - v_{\alpha}/v_A$ plane for two distinct situations of (a) $T_{i\perp}/T_{i\parallel} \leq 1$ and (b) $T_{i\perp}/T_{i\parallel} \geq 1$. In Figure 4(a) the solid, dashed and dotted lines represent the PM/W, OA/IC and BM/W waves, respectively, and the black, red and blue lines correspond to different proton temperature anisotropies $T_{i\perp}/T_{i\parallel} = 0.25, 0.5$ and 1 , respectively, and in Figure 4(b) the solid, dashed, dotted and dotted-dashed lines represent the PM/W, OA/IC, PA/IC and mirror waves, respectively, and the black, red and blue lines correspond to different proton temperature anisotropies $T_{i\perp}/T_{i\parallel} = 1, 1.5$ and 2 , respectively. The plasma parameters are $n_{\alpha} = 0.05n_e$, $T_{\alpha\parallel} = 4T_{e\parallel} = 4T_{i\parallel}$ and $4T_{e\perp} = T_{\alpha\perp} = 4T_{i\perp}$.

waves. At $T_{i\perp}/T_{i\parallel} = 1$, both PM/W and OA/IC waves can be induced by the alpha beams, but they have different unstable regimes. The OA/IC wave is more likely to excite at $\beta_{e\parallel} < 0.5$, while the PM/W wave is more inclined to arise at $\beta_{e\parallel} > 0.5$, which is in agreement with previous results in Gary et al. (2000a, 2000b). As $T_{i\perp}/T_{i\parallel}$ decreases from 1 to 0.25, the threshold velocity of both OA/IC and PM/W waves obviously decreases, especially for the OA/IC wave at $\beta_{e\parallel} > 2$. Also, the

BM/W wave appears at $T_{i\perp}/T_{i\parallel} = 0.25$ and 0.5 , implying that the proton temperature anisotropy with $T_{i\perp}/T_{i\parallel} < 1$ can provide additional free energy contributing to the generation and growth of BM/W waves. The threshold condition of the BM/W wave is reduced to a lower v_{α}/v_A and a lower $\beta_{e\parallel}$ at $T_{i\perp}/T_{i\parallel} = 0.25$. Besides, for the cases of $T_{i\perp}/T_{i\parallel} \geq 1$ shown in Figure 4(b), four types of waves exist: PM/W, OA/IC, PA/IC and mirror waves. As $T_{i\perp}/T_{i\parallel}$ increases from 1 to 2, the

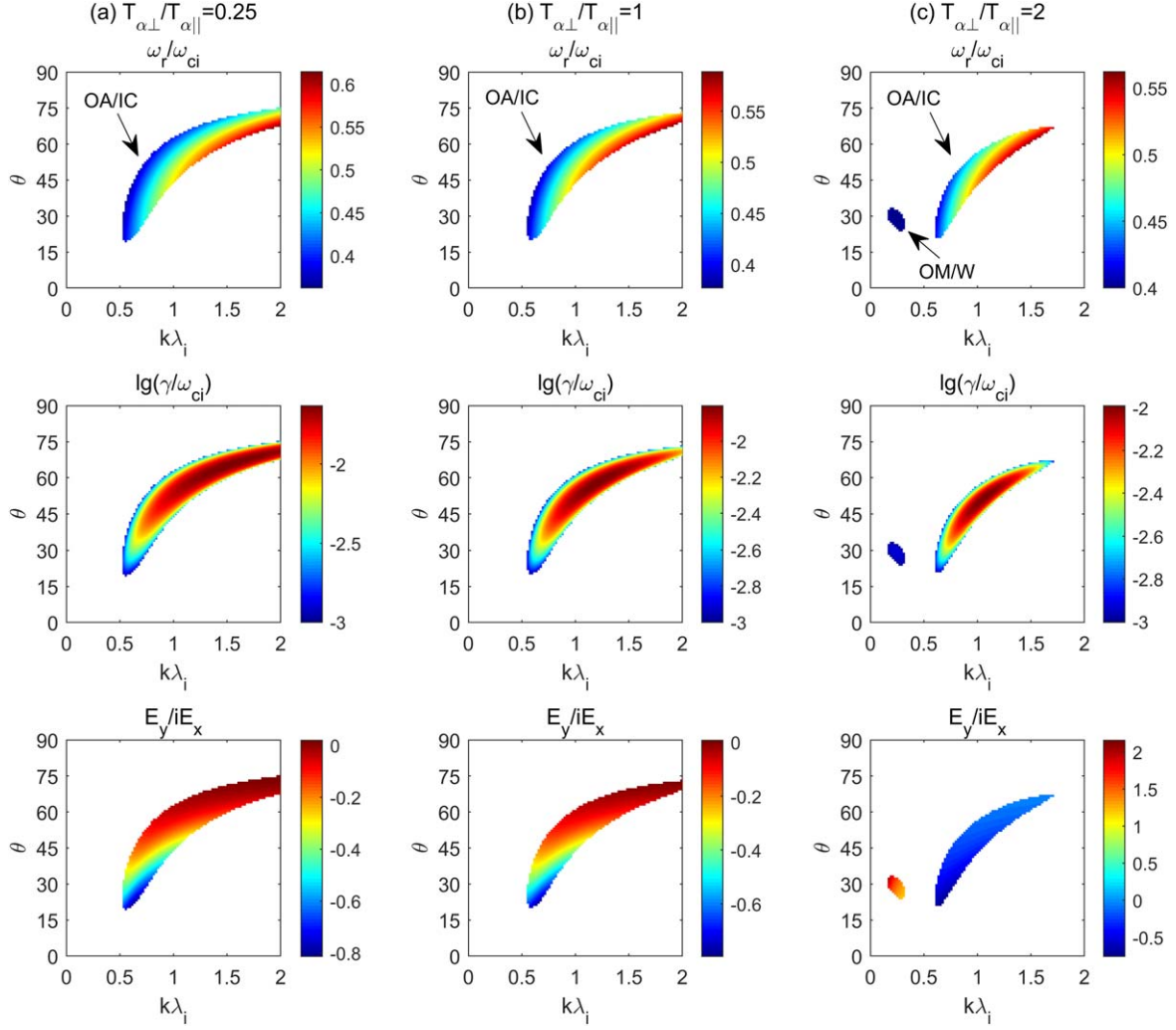


Figure 5. The distribution of the real frequency ω_r/ω_{ci} (top), growth rate γ/ω_{ci} (middle) and polarization E_y/iE_x (bottom) in the plane of the propagation angle θ and normalized wavenumber $k\lambda_i$ for the OA/IC and OM/W waves in the plasma with low-beta $\beta_{e\parallel} = 0.1$, where the left, middle and right panels correspond to different alpha temperature anisotropies of (a) $T_{\alpha\perp}/T_{\alpha\parallel} = 0.25$, (b) 1 and (c) 2. The additional plasma parameters are given as $n_\alpha = 0.05n_e$, $v_\alpha = 1.5v_A$, $T_{\alpha\parallel} = 4T_{e\parallel} = 4T_{i\parallel}$ and $4T_{e\perp} = 4T_{i\perp} = T_{\alpha\perp}$.

threshold v_α/v_A of PM/W waves increases, while that of OA/IC waves first increases slightly then decreases sharply. Moreover, the presence of $T_{i\perp}/T_{i\parallel} > 1$ leads to lower thresholds v_α/v_A for the PA/IC and mirror waves, which can be reduced to near or below v_A .

4. Effects of Alpha Temperature Anisotropy on Alpha Beam Instability

We investigate the alpha-beam instability associated with the alpha temperature anisotropy and perform the effects of alpha temperature anisotropy on these instabilities at arbitrary propagation angles with respect to \mathbf{B}_0 . In this section, we assume the alpha beam with an anisotropic temperature, while

the background proton and electron are taken as with an isotropic temperature.

Figure 5 shows the distribution of the dispersion relations and polarization properties in the plane of the propagation angle θ and normalized wavenumber $k\lambda_i$ for the OA/IC wave in the plasma with low-beta $\beta_{e\parallel} = 0.1$, where panels (a), (b) and (c) correspond to different alpha temperature anisotropies $T_{\alpha\perp}/T_{\alpha\parallel} = 0.25, 1$ and 2 , respectively. The plasma parameters are $n_\alpha/n_e = 0.05$, $v_\alpha/v_A = 1.5$, $4T_{i\parallel} = 4T_{e\parallel} = T_{\alpha\parallel}$ and $4T_{i\perp} = 4T_{e\perp} = T_{\alpha\perp}$. From Figure 5, it can be seen that only the OA/IC wave survives at $\beta_{e\parallel} = 0.1$. Moreover, the real frequency, growth rate and polarization of the OA/IC wave are insensitive to the alpha temperature anisotropy $T_{\alpha\perp}/T_{\alpha\parallel}$, implying that the influence of

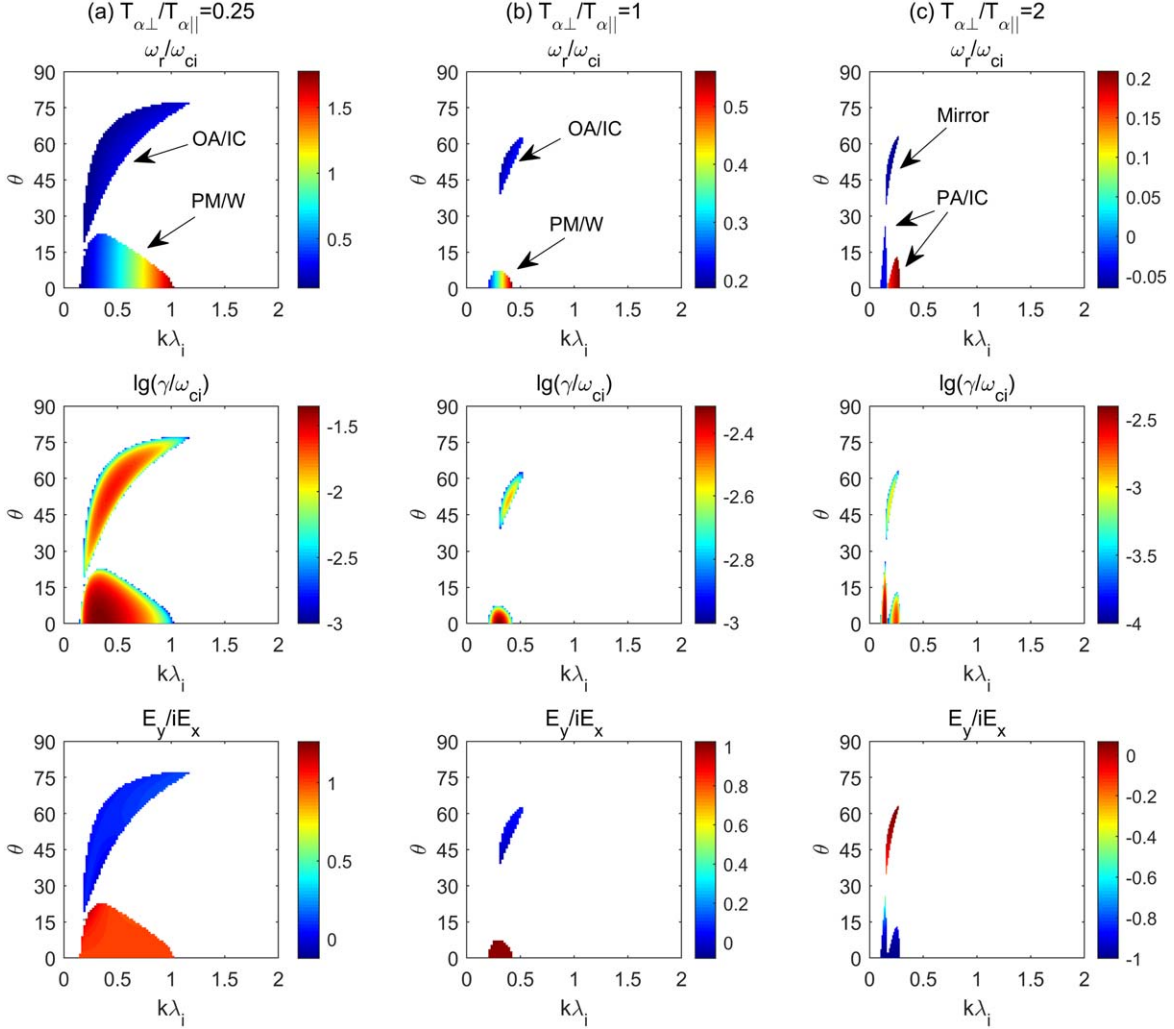


Figure 6. The distribution of the real frequency ω_r/ω_{ci} (top), growth rate γ/ω_{ci} (middle) and polarization E_y/iE_x (bottom) in the plane of the propagation angle θ and normalized wavenumber $k\lambda_i$ for the OA/IC, PM/W, PA/IC and mirror waves in the plasma with high-beta $\beta_{e\parallel} = 1.5$, where the left, middle and right panels correspond to different alpha temperature anisotropies of (a) $T_{\alpha\perp}/T_{\alpha\parallel} = 0.25$, (b) 1 and (c) 2. The additional plasma parameters are given as $n_\alpha = 0.05n_e$, $v_\alpha = 1.5v_A$, $T_{\alpha\parallel} = 4T_{e\parallel} = 4T_{i\parallel}$ and $4T_{e\perp} = 4T_{i\perp} = T_{\alpha\perp}$.

$T_{\alpha\perp}/T_{\alpha\parallel}$ on wave properties of OA/IC waves is minor at $\beta_{e\parallel} = 0.1$.

Figure 6 shows the distribution of the dispersion relations and polarization properties in the plane of the propagation angle θ and normalized wavenumber $k\lambda_i$ for the PM/W, OA/IC, PA/IC and mirror waves in the plasma with high-beta $\beta_{e\parallel} = 1.5$. Here planes (a), (b) and (c) correspond to different alpha temperature anisotropies $T_{\alpha\perp}/T_{\alpha\parallel} = 0.25$, 1 and 2, respectively. From Figure 6, one finds that the PM/W wave dominates in the unstable region at $\theta \leq 10^\circ$, while the OA/IC wave distributes at $40^\circ \leq \theta \leq 60^\circ$ when $T_{\alpha\perp}/T_{\alpha\parallel} = 1$, which is consistent with the results of Gary et al. (2000a, 2000b). Moreover, the unstable ranges of θ and $k\lambda_i$ of PM/W and OA/IC waves strongly depend on the alpha temperature anisotropy.

For example, as $T_{\alpha\perp}/T_{\alpha\parallel} = 1$ (0.25), the propagation angle is $\theta \leq 10^\circ$ ($\theta \leq 20^\circ$) for the PM/W wave and $40^\circ \leq \theta \leq 60^\circ$ ($30^\circ \leq \theta \leq 70^\circ$) for the OA/IC wave. As $T_{\alpha\perp}/T_{\alpha\parallel} = 2$, the PA/IC and mirror waves are unstable, while the PM/W and OA/IC waves disappear. This indicates that the presence of the anisotropic alpha beams with $T_{\alpha\perp}/T_{\alpha\parallel} > 1$ can lead to an enhancement of the growth of PA/IC and mirror waves, but an inhibition of the growth of the PM/W and OA/IC waves.

To understand more general wave properties, we present in Figure 7 the distributions of the dispersion relations (ω_r/ω_{ci} and $\gamma_{\max}/\omega_{ci}$) in the plane of the parallel electron beta $\beta_{e\parallel}$ and the alpha-beam drift velocity v_α/v_A for different values of alpha temperature anisotropy $T_{\alpha\perp}/T_{\alpha\parallel} = 0.25$ ((a), (d)), 1 ((b), (e)) and 2 ((c), (f)). Here panels (a)–(c) represent PM/W and PA/IC waves at

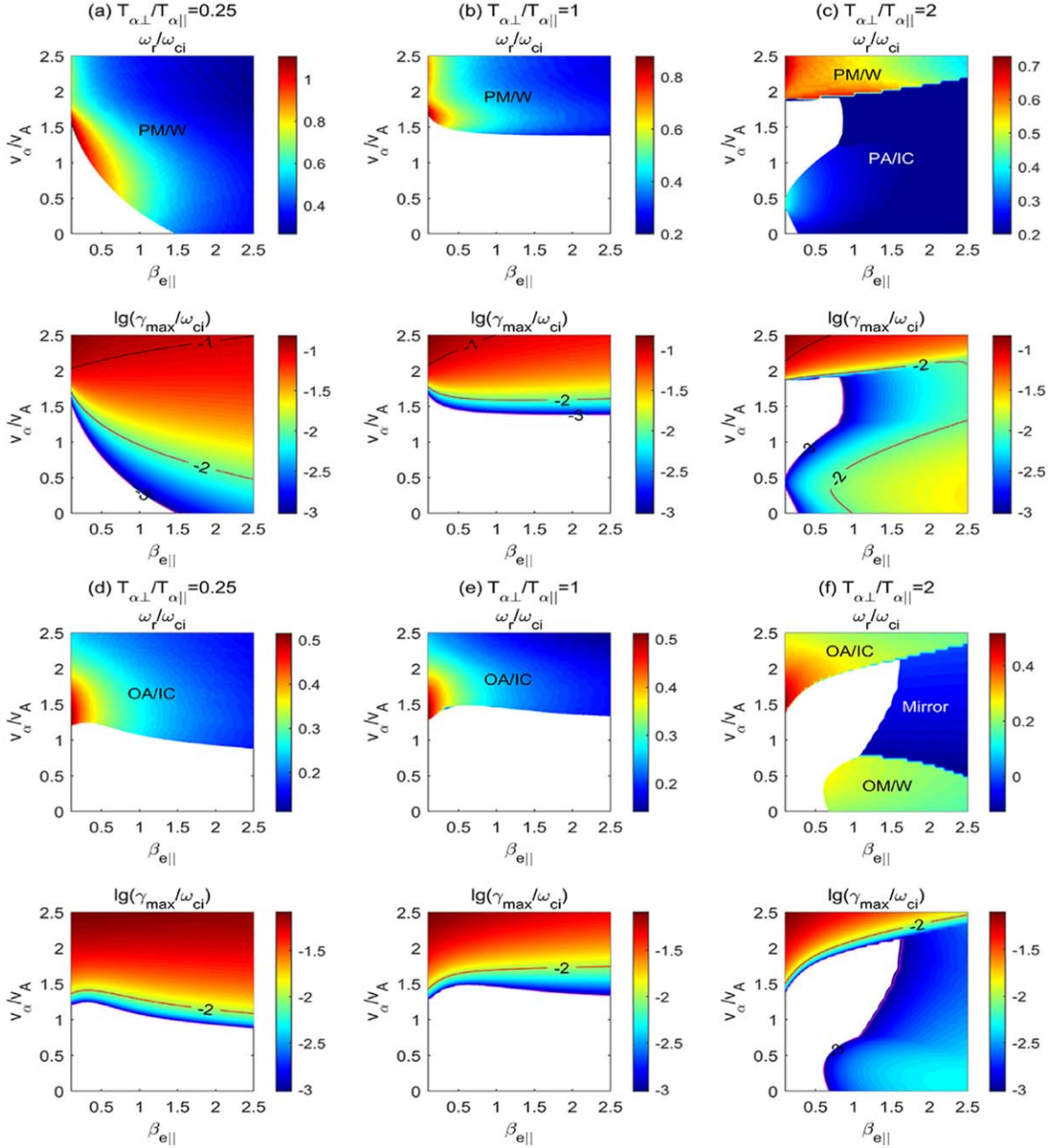


Figure 7. The distribution of the maximum growth rate $\gamma_{\max}/\omega_{ci}$ and corresponding real frequency ω_r/ω_{ci} in the plane of the parallel electron beta $\beta_{e\parallel}$ and alpha-proton drift velocity v_{α}/v_A for the PM/W and PA/IC waves at $\theta = 0$ ((a)–(c)) and for the OA/IC, OM/W and mirror waves at $\theta = 55^\circ$ ((d)–(f)). The left, middle and right panels correspond to different alpha temperature anisotropies of $T_{\alpha\perp}/T_{\alpha\parallel} = 0.25$ ((a), (d)), 1 ((b), (e)) and 2 ((c), (f)). In the maximum growth rate panels, the values of $\gamma_{\max}/\omega_{ci} = 10^{-3}$, 10^{-2} and 10^{-1} are marked with the black solid line. The additional plasma parameters are adopted as $n_{\alpha} = 0.05n_e$, $T_{\alpha\parallel} = 4T_{e\parallel} = 4T_{i\parallel}$ and $4T_{e\perp} = 4T_{i\perp} = T_{\alpha\perp}$.

the parallel propagation case of $\theta = 0$, and panels (d)–(f) stand for the OA/IC, oblique magnetosonic/whistler (OM/W) and mirror waves at the oblique propagation case of $\theta = 55^\circ$. In the maximum growth rate distributions, the black solid lines correspond to the contour values of $\gamma_{\max}/\omega_{ci} = 10^{-3}$, 10^{-2} and 10^{-1} , respectively. For parallel propagation cases shown in Figures 7(a)–(c), there are

two kinds of waves, i.e., the PM/W and PA/IC waves. For oblique propagation cases shown in Figures 7(d)–(f), three kinds of waves exist, that is, the OA/IC, OM/W, and mirror waves. These waves distribute in different plasma parameter regimes.

As shown in Figures 7(a)–(c), the PM/W wave has an unstable region wider at $T_{\alpha\perp}/T_{\alpha\parallel} = 0.25$ than at $T_{\alpha\perp}/T_{\alpha\parallel} = 1$.

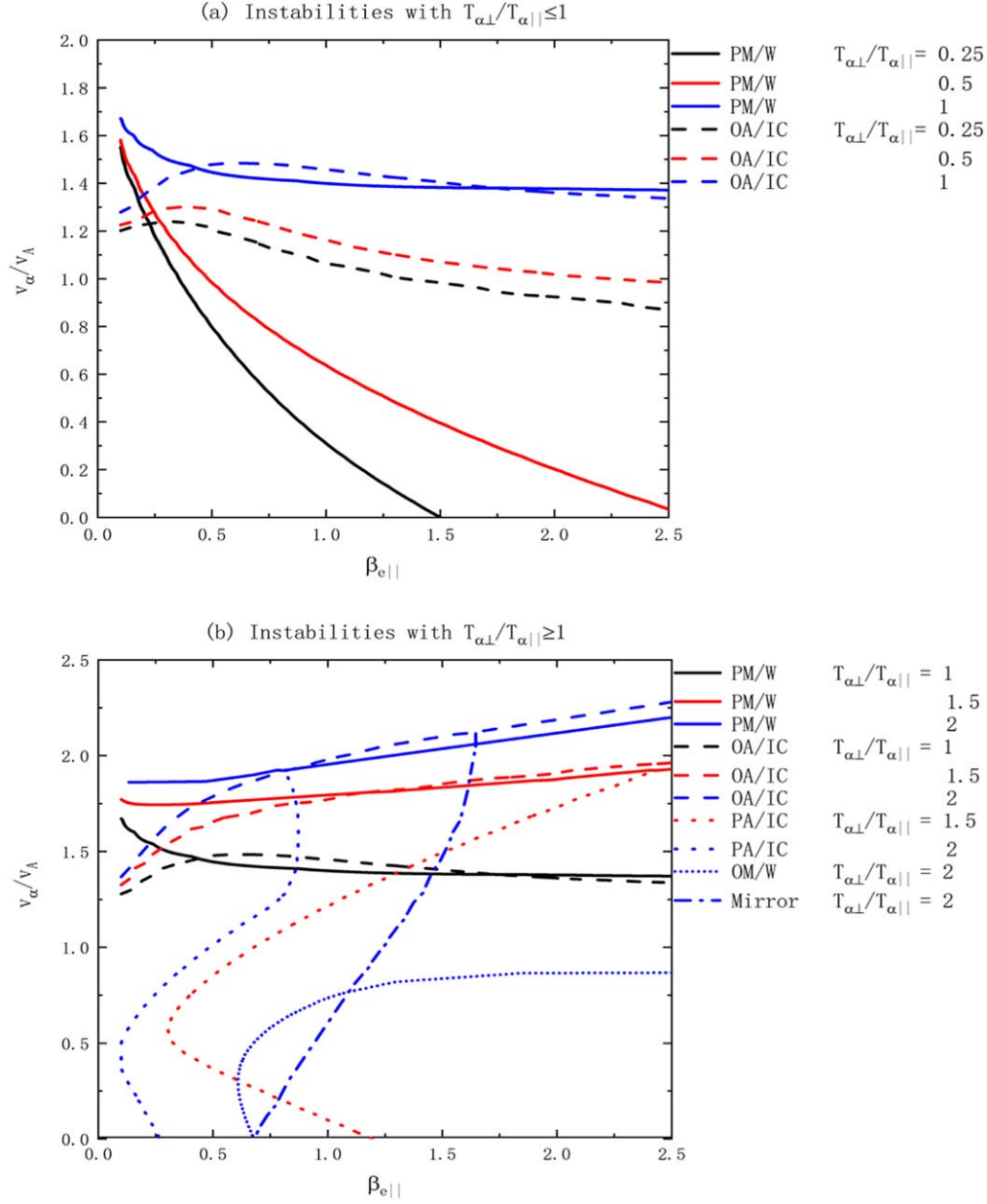


Figure 8. The instability threshold in the $\beta_{e\parallel}$ - v_{α}/v_A plane for two distinct situations of (a) $T_{\alpha\perp}/T_{\alpha\parallel} \leq 1$ and (b) $T_{\alpha\perp}/T_{\alpha\parallel} \geq 1$. In Figure 8(a) the solid and dashed lines represent the PM/W and OA/IC waves, respectively, and the black, red and blue lines correspond to different alpha temperature anisotropies $T_{i\perp}/T_{i\parallel} = 0.25, 0.5$ and 1 , respectively. In Figure 8(b) the solid, dashed, dotted, thick-dotted and dotted-dashed lines represent the PM/W, OA/IC, PA/IC, OM/W and mirror waves, respectively, and the black, red and blue lines correspond to different alpha temperature anisotropies $T_{\alpha\perp}/T_{\alpha\parallel} = 1, 1.5$ and 2 , respectively. The plasma parameters are adopted as $n_{\alpha} = 0.05n_e$, $T_{\alpha\parallel} = 4T_{e\parallel} = 4T_{i\parallel}$ and $4T_{e\perp} = 4T_{i\perp} = T_{\alpha\perp}$.

As $T_{\alpha\perp}/T_{\alpha\parallel} = 2$, the PA/IC wave arises, which extends to lower threshold conditions (i.e., $v_{\alpha}/v_A < 1$). In addition, the oblique waves are further presented in Figures 7(d)–(f). Compared with the $T_{\alpha\perp}/T_{\alpha\parallel} = 1$ case, the threshold v_{α}/v_A of the OA/IC wave can extend to a lower value in the case of $T_{\alpha\perp}/T_{\alpha\parallel} = 0.25$ (i.e., $v_{\alpha}/v_A \leq 1$ for $\beta_{e\parallel} \geq 1$). Moreover, besides the OA/IC wave, both mirror and OM/W waves can

be excited at $T_{\alpha\perp}/T_{\alpha\parallel} = 2$. The mirror wave dominates in the higher velocity regime of $0.8 < v_{\alpha}/v_A < 2$, while the OM/W wave dominates in the lower velocity regime of $v_{\alpha}/v_A < 0.8$.

In addition, we discuss the possible relevance of the alpha temperature anisotropy to the threshold conditions. Figure 8 displays the instability thresholds of the normalized alpha-beam drift velocity v_{α}/v_A versus the parallel electron beta $\beta_{e\parallel}$,

where the top and bottom panels correspond to two different situations of (a) $T_{\alpha\perp}/T_{\alpha\parallel} \leq 1$ and (b) ≥ 1 , respectively. In Figure 8(a) the solid and dashed lines correspond to the PM/W and OA/IC waves, and in Figure 8(b) five types of lines represent the PM/W, OA/IC, PA/IC, OM/W and mirror waves, respectively. For an excess of parallel temperature $T_{\alpha\perp}/T_{\alpha\parallel} \leq 1$ shown in Figure 8(a), it can be found that the threshold velocities of both PM/W and OA/IC waves are shifted to lower values as $T_{\alpha\perp}/T_{\alpha\parallel}$ decreases. This tide is more prominent for the PM/W wave at $\beta_{e\parallel} > 0.5$. The threshold velocity is $v_{\alpha}/v_A \leq 1$ (1.2) for the PM/W wave (the OA/IC wave) when $T_{\alpha\perp}/T_{\alpha\parallel} \leq 0.5$ and $\beta_{e\parallel} \geq 1$. On the other hand, for an excess of perpendicular temperature $T_{\alpha\perp}/T_{\alpha\parallel} \geq 1$ presented in Figure 8(b), the threshold velocities of both PM/W and OA/IC waves increase as $T_{\alpha\perp}/T_{\alpha\parallel}$ increases. As $T_{\alpha\perp}/T_{\alpha\parallel} = 2$, the PA/IC, OM/W, and mirror waves arise, and their instability thresholds extend to lower values (i.e., $v_{\alpha}/v_A < 1$). This implies that the presence of the anisotropic alpha beams with $T_{\alpha\perp}/T_{\alpha\parallel} > 1$ can lead to a broader unstable region at a lower $\beta_{e\parallel}$ and/or lower v_{α}/v_A .

5. Discussion and Conclusion

In-situ observations by space satellites have revealed that the alpha beams often stream faster than the background protons, and the drift velocity between two components is typically less than the local Alfvén velocity (Marsch et al. 1982a; Marsch & Livi 1987; Steinberg et al. 1996; Neugebauer et al. 1996; Feldman et al. 1996; Verniero et al. 2020). Because the local Alfvén velocity decreases with the increase of the heliocentric distance (Marsch et al. 1982b), the observed limitation of the alpha beams with $v_{\alpha}/v_A \leq 1$ implies that the drift velocity of the alpha beams v_{α} is continuously reduced when the solar wind flows from the Sun into the interplanetary space (Chandran et al. 2013; Alterman et al. 2018). The alpha beam instability has been proposed to be responsible for decelerating the alpha-beam drift velocity in the solar wind (Revathy 1978; Gary et al. 2000a, 2000b). However, there is still no consensus on the details of deceleration processes for the solar wind alpha beams. Also, the effects of the ion temperature anisotropy on the alpha beam instability have not been examined. In this study, we investigate the properties of the alpha beam instability in the presence of both proton and alpha temperature anisotropies in the solar wind and consider the effects of $T_{i\perp}/T_{i\parallel}$ and $T_{\alpha\perp}/T_{\alpha\parallel}$ on these instabilities at arbitrary propagation angles.

It is found that the wave dispersion relations and polarization properties of ω_r/ω_{ci} , γ/ω_{ci} and E_y/iE_x are strongly dependent on $T_{i\perp}/T_{i\parallel}$, $T_{\alpha\perp}/T_{\alpha\parallel}$ and $\beta_{e\parallel}$. Moreover, the effects of $T_{i\perp}/T_{i\parallel}$ and $T_{\alpha\perp}/T_{\alpha\parallel}$ on these waves are minor in the region with low-beta $\beta_{e\parallel} < 1$, but obvious in the region with high-beta $\beta_{e\parallel} \geq 1$. For the condition of both proton temperature anisotropy and alpha beam, there exist different types of unstable modes, i.e., the PM/W, BM/W and OA/IC waves at $T_{i\perp}/T_{i\parallel} < 1$ and the PM/W, PA/IC, OA/IC and mirror waves at $T_{i\perp}/T_{i\parallel} > 1$. For

$T_{i\perp}/T_{i\parallel} < 1$, as $T_{i\perp}/T_{i\parallel}$ decreases, the growth rates of the BM/W and OA/IC waves are enhanced by $T_{i\perp}/T_{i\parallel}$, and their instability thresholds of both two waves are extended to a lower v_{α}/v_A and a lower $\beta_{e\parallel}$ at the propagation angle of $\theta = 0$ and 55° , respectively. For $T_{i\perp}/T_{i\parallel} > 1$, as $T_{i\perp}/T_{i\parallel}$ increases, the instability thresholds of the PA/IC, OA/IC and mirror waves are diverted to a lower v_{α}/v_A and a lower $\beta_{e\parallel}$.

For the condition of both alpha temperature anisotropy and alpha beam, there are different kinds of unstable modes: the PM/W and OA/IC waves at $T_{\alpha\perp}/T_{\alpha\parallel} < 1$ and the PM/W, OA/IC, PA/IC, OM/W and mirror waves at $T_{\alpha\perp}/T_{\alpha\parallel} > 1$. For $T_{\alpha\perp}/T_{\alpha\parallel} < 1$, with the decrease of $T_{\alpha\perp}/T_{\alpha\parallel}$, the growth rates of the PM/W and OA/IC waves increase, and the threshold conditions of two waves are extended to a smaller v_{α}/v_A , especially for the PM/W wave at $\beta_{e\parallel} > 0.5$. For $T_{\alpha\perp}/T_{\alpha\parallel} > 1$, with the increase of $T_{\alpha\perp}/T_{\alpha\parallel}$, the growth rates of the PM/W and the OA/IC waves decrease, while those of the PA/IC, OM/W and mirror waves increase. Moreover, the unstable regimes of the PA/IC, OM/W and mirror wave are enlarged to a lower v_{α}/v_A and a lower $\beta_{e\parallel}$.

In addition, we compare the present results with those of the previous studies in Gary et al. (2000a, 2000b). The existence of the temperature anisotropy of the proton and alpha particles can lead to not only the enhanced alpha beam instabilities, but also the excitation of extra wave modes. The proton and/or alpha temperature anisotropy exerts a strong influence on the threshold of the alpha beam instabilities, resulting in a larger growth rate and a lower threshold velocity. Therefore, the alpha beam instability accompanied with the proton and/or alpha temperature anisotropy may reduce the alpha-beam drift velocity to near or less than the local Alfvén velocity, which shows a good fit to the observations in the solar wind.

In summary, our physical model could give a rational explanation for the alpha-beam deceleration in the solar wind. When the solar wind plasma flows into the interplanetary space, the alpha-beam drift velocity v_{α} does not vary obviously, but the local Alfvén velocity v_A certainly decreases, which leads to an increase of the normalized drift velocity v_{α}/v_A . As v_{α}/v_A exceeds the threshold of the alpha beam instability, the beam energy is transferred to the wave energy via the OA/IC and PM/W wave excitation. However, when $v_{\alpha}/v_A < 1.5$, the alpha beam instability accompanied with proton and alpha temperature anisotropies could work in concert to deceleration alpha beams because its threshold condition undergoes major changes in the presence of the anisotropic proton and alpha. In general, both the proton and alpha temperature anisotropies are common intrinsic phenomena in the solar wind (Yoon et al. 2019). In plasma environments with $T_{i\perp}/T_{i\parallel} \neq 1$, the deceleration of the alpha beams is governed by the BM/W and OA/IC waves at $T_{i\perp}/T_{i\parallel} < 1$ and by the PA/IC, OA/IC and mirror waves at $T_{i\perp}/T_{i\parallel} > 1$. While in plasma environments with $T_{\alpha\perp}/T_{\alpha\parallel} \neq 1$, the dissipation of the alpha beams is regulated by the PM/W wave at $T_{\alpha\perp}/T_{\alpha\parallel} < 1$ and by the PA/IC, OM/W and mirror waves at $T_{\alpha\perp}/T_{\alpha\parallel} > 1$. The presence of both the proton

and alpha temperature anisotropies further limits the alpha-beam drift velocity to less than the local Alfvén velocity, which shows a good agreement with the solar wind observations. Our results are potentially important for comprehending the deceleration and evolution mechanism of alpha particles in the solar wind.

Acknowledgments

This work was supported by the National Natural Science Foundation of China under grants 12103018, 11690034, and 12075084. L. Xiang also was supported by the Science and Technology Innovation Program of Hunan Province (2020RC2049). We give special thanks to Dr. J. F. Tang at XAO for the valuable suggestions.

References

- Alterman, B. L., Kasper, J. C., Stevens, M. L., & Koval, A. 2018, *ApJ*, **864**, 112
- Bale, S. D., Kasper, J. C., Howes, G. G., et al. 2009, *PhRvL*, **103**, 211101
- Bame, S. J., Asbridge, J. R., Feldman, W. C., & Gosling, J. T. 1977, *JGRA*, **82**, 1487
- Borovsky, J. E. 2016, *JGRA*, **121**, 5055
- Bourouaine, S., Verscharen, D., Chandran, B. D. G., Maruca, B. A., & Kasper, J. C. 2013, *ApJL*, **777**, L3
- Chandran, B. D. G., Verscharen, D., Quataert, E., et al. 2013, *ApJ*, **776**, 45
- Chen, L., & Wu, D. J. 2012, *ApJ*, **754**, 123
- Chen, L., Wu, D. J., Xiang, L., et al. 2020, *ApJ*, **904**, 193
- Chew, G. F., Goldberger, M. L., & Low, F. E. 1956, *RSPSA*, **236**, 112
- Ebert, R. W., McComas, D. J., Elliott, H. A., Forsyth, R. J., & Gosling, J. T. 2009, *JGRA*, **114**, A01109
- Feldman, W. C., Barraclough, B. L., Phillips, J. L., & Wang, Y. M. 1996, *A&A*, **316**, 355
- Gary, S. P., Goldstein, B. E., & Steinberg, J. T. 2001, *JGRA*, **106**, 24955
- Gary, S. P., Jian, L. K., Broiles, T. W., et al. 2016, *JGRA*, **121**, 30
- Gary, S. P., Yin, L., Winske, D., & Reisenfeld, D. B. 2000a, *JGRA*, **105**, 20989
- Gary, S. P., Yin, L., Winske, D., & Reisenfeld, D. B. 2000b, *GeoRL*, **27**, 1355
- Hellinger, P., Trávníček, P., Kasper, J. C., & Lazarus, A. J. 2006, *GeoRL*, **33**, L09101
- Huang, J., Kasper, J. C., Vech, D., et al. 2020, *ApJS*, **246**, 70
- Jian, L. K., Moya, P. S., Viñas, A. F., & Stevens, M. 2016, in AIP Conf. Ser., 1720, Solar Wind 14 (Melville, NY: AIP) 040007
- Kasper, J. C., Lazarus, A. J., & Gary, S. P. 2008, in AIP Conf. Ser., 679, 538
- Kasper, J. C., Lazarus, A. J., Gary, S. P., & Szabo, A. 2003, in Institute of Physics Conf. Ser., 679, ed. M. Velli, 538
- Li, B., & Li, X. 2006, *A&A*, **456**, 359
- Lu, Q., Du, A., & Li, X. 2009, *PhPI*, **16**, 042901
- Markovskii, S. A., Chandran, B. D. G., & Vasquez, B. J. 2019, *ApJ*, **870**, 121
- Marsch, E. 2012, *SSRv*, **172**, 23
- Marsch, E., & Livi, S. 1987, *JGRA*, **92**, 7263
- Marsch, E., & Richter, A. K. 1984, *JGRA*, **89**, 5386
- Marsch, E., Rosenbauer, H., Schwenn, R., Muehlhaeuser, K. H., & Neubauer, F. M. 1982a, *JGRA*, **87**, 35
- Marsch, E., Schwenn, R., Rosenbauer, H., et al. 1982b, *JGRA*, **87**, 52
- Maruca, B. A., Kasper, J. C., & Gary, S. P. 2012, *ApJ*, **748**, 137
- Neugebauer, M., Goldstein, B. E., Smith, E. J., & Feldman, W. C. 1996, *JGRA*, **101**, 17047
- Ofman, L. 2019, *SoPh*, **294**, 51
- Pizzo, V., Schwenn, R., Marsch, E., et al. 1983, *ApJ*, **271**, 335
- Rehman, M. A., Shaaban, S. M., Yoon, P. H., Lazar, M., & Poedts, S. 2020, *Ap&SS*, **365**, 107
- Reisenfeld, D. B., Gary, S. P., Gosling, J. T., et al. 2001, *JGRA*, **106**, 5693
- Revathy, P. 1978, *JGRA*, **83**, 5750
- Roenmark, K. 1982, Waves in Homogeneous, Anisotropic Multicomponent Plasmas (WHAMP), Report, 179
- Seough, J., Yoon, P. H., Kim, K.-H., & Lee, D.-H. 2013, *PhRvL*, **110**, 071103
- Steinberg, J. T., Lazarus, A. J., Ogilvie, K. W., Lepping, R., & Byrnes, J. 1996, *GeoRL*, **23**, 1183
- Stix, T. H. 1992, Waves in plasmas (New York: American Institute of Physics)
- Sugiyama, H., Singh, S., Omura, Y., et al. 2015, *JGRA*, **120**, 8426
- Sun, H., Zhao, J., Liu, W., Xie, H., & Wu, D. 2020, *ApJ*, **902**, 59
- Sun, H., Zhao, J., Xie, H., & Wu, D. 2019, *ApJ*, **884**, 44
- Đurovcová, T., Němeček, Z., & Šafránková, J. 2019, *ApJ*, **873**, 24
- Verniero, J. L., Larson, D. E., Livi, R., et al. 2020, *ApJS*, **248**, 5
- Verscharen, D., Bourouaine, S., & Chandran, B. D. G. 2013a, *ApJ*, **773**, 163
- Verscharen, D., Bourouaine, S., Chandran, B. D. G., & Maruca, B. A. 2013b, *ApJ*, **773**, 8
- Verscharen, D., Chandran, B. D. G., Bourouaine, S., & Hollweg, J. V. 2015, *ApJ*, **806**, 157
- Wu, D. J. 2012, Kinetic Alfvén Waves: Theory, Experience, and Application (Beijing: Science Press)
- Xiang, L., Lee, K. H., Wu, D. J., & Lee, L. C. 2020, *ApJ*, **899**, 61
- Xiang, L., Lee, K. H., Wu, D. J., Yu, H. W., & Lee, L. C. 2021, *ApJ*, **916**, 30
- Xiang, L., Wu, D. J., & Chen, L. 2018, *ApJ*, **869**, 64
- Xie, H., & Xiao, Y. 2016, *PIST*, **18**, 97
- Xie, H.-s. 2019, *CoPhC*, **244**, 343
- Yoon, P. H., Seough, J., Salem, C. S., & Klein, K. G. 2019, *PhRvL*, **123**, 145101